



Cite this: *Green Chem.*, 2018, **20**, 2984

Received 8th May 2018,
Accepted 11th June 2018

DOI: 10.1039/c8gc01436a

rsc.li/greenchem

Green and continuous route to assemble lateral nanodimensional graphitic oxide composites without process interruption†

Bijay Kumar Poudel,^a Kyung-Oh Doh^{*b} and Jeong Hoon Byeon  ^{*a}

A single-pass process was developed to continuously assemble lateral nanoscaled iron (pure iron and iron oxide-hydroxide)-decorated graphitic oxide conjugated with doxorubicin and polyethylene glycol (IDGO@DOX-PEG) flakes. The resulting flakes were employed for magneto- and photo-thermal therapies as well as magnetic resonance (MR) imaging as a theranostic nanosystem. The lateral nanoscaled GO flakes were primarily biocompatible and suitable to suppress burst DOX release because of abundant oxygenated plane and edges for DOX conjugation, and the fully nanoscale system was further feasible for near-infrared induced chemophototherapy to kill HeLa cells. The decorated iron nanoparticles exhibited a superparamagnetic behavior. IDGO@DOX-PEG flakes, thus, further demonstrated effective chemo-magnetotherapy under alternating magnetic field as well as contrasting activity for MR imaging. This study offers a new and generalizable concept to continuously assemble composite GO nanoflakes for theranostic nanomedicine which usually requires complicated hazardous chemistries and multiple posttreatments.

Because of its unique physicochemical properties, graphitic oxide (GO) and its derivatives have been widely employed in biomedical fields (>60% toward biomedical applications of all GO-related researches),^{1,2} although there are challenging issues for successful applications.³ In particular, the presence of functional groups of epoxy (C–O–C), hydroxyl (OH), carbonyl (C=O), and carboxyl (COOH) on its basal plane and edges, which makes GO hydrophilic, can provide anchors to conjugate with drug molecules and inorganic nanoparticles for theranostic nanomedicines (*i.e.*, stimulating drug release and providing contrast imaging under external physical stimuli for cancer detection, diagnosis, and treatment).^{4–6} Therefore, numerous studies have recently been introduced to chemically

modify and combine GO with various functional components, such as polymers and inorganic nanoparticles.^{7–10}

Even though the GO composite has biocompatibility and achieves great improvements in theranostic efficacy,¹¹ preparation of the GO composite generally requires time-consuming and complicated reactions as well as a large amounts of toxic chemicals.^{6,12} The lack of appropriate assembly devices and systems for the GO composite may impede the development of suitable nanoplateforms for realizing theranostic nanomedicines.¹³ Exploring efficient protocols for preparing GO composite has also been introduced.¹⁴ However, the effort was still based on multistep wet chemistries and required multiple separations, purifications, or posttreatments. Moreover, the conventional structure of the GO composite is based on lateral microdimensional GO. Therefore, high toxicities, inflammations, and limited cellular internalization modes (mostly phagocytosis) could be promoted for their efficient translation.^{13,15}

On this account, the present work introduces a simple and green assembly of lateral nanoscaled iron (pure iron and iron oxide-hydroxide)-decorated GO (IDGO) in a single-pass continuous configuration. Carbon-encapsulated iron (CEI) nanoparticles were re-organized as IDGO *via* a gas–liquid–gas route without process interruption (Fig. 1). To simultaneously supply precursors for lateral nanoscaled GO flakes and iron nanoparticles, heterogeneous spark ablation between iron and graphite rods was adopted to prepare CEI nanoparticles first under nitrogen gas flow (process 1). The CEI particles were directly dispersed in a K₂FeO₄ + H₂O₂ solution *via* ultrasonic cavitation.¹⁶ Subsequent separation of the iron core and graphitic shell was accelerated *via* ultrasound irradiation.¹⁷ The ultrasound treatment not only derived rapid bubble (CEI particles in nitrogen gas) cavitation (*i.e.*, hydrosolization of CEI particles) before the bubbles move to the free surface of the solution but also enhanced production of GO nanoflakes and successive decoration of iron nanoparticles on GO flakes through sonochemistry within 2 min of CEI particle residence time (process 2). The formed IDGO was suspended as droplets in gas *via* Collision atomization (first), which passed through a

^aSchool of Mechanical Engineering, Yeungnam University, Gyeongsan 38541, Republic of Korea. E-mail: postjb@yu.ac.kr

^bCollege of Medicine, Yeungnam University, Daegu 42415, Republic of Korea. E-mail: kodoh@ynu.ac.kr

†Electronic supplementary information (ESI) available. See DOI: 10.1039/c8gc01436a

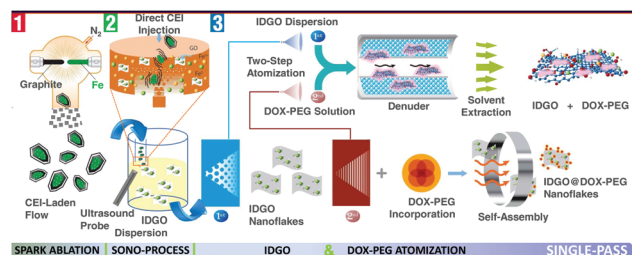


Fig. 1 Schematic of the single-pass assembly of IDGO@DOX-PEG nanoflakes. Ambient spark ablation between iron and graphite rods produced iron and carbon vapors, and these vapors were subsequently condensed into CEI nanoparticles through catalytic graphitization on the iron particle surface (process 1). The CEI particle-laden nitrogen gas flow was directly injected (because of negligible gravitational sedimentation of nanoscaled particles) into the solution ($K_2FeO_4 + H_2O_2$ in de-ionized water) containing an ultrasound probe to be exfoliated and subsequently incorporated with iron nanoparticles (*i.e.*, IDGO) (process 2). These IDGO flakes were eventually incorporated with DOX-PEG droplets in a single-pass configuration during solvent extraction from the droplets (process 3).

denuder to remove solvent from the droplets. The IDGO-flake-laden nitrogen flow was injected into another atomizer (second) filled with ethanolic doxorubicin-polyethylene glycol (DOX-PEG) solution to generate hybrid droplets containing IDGO and DOX-PEG. The solvent of the droplets was extracted in a heated tubular reactor, forming lateral nanoscaled IDGO@DOX-PEG flakes in a single-pass configuration (Fig. S1, ESI†) (process 3). The controlled DOX release property and cellular internalization of IDGO@DOX-PEG flakes were first examined, including biocompatibility. Magneto- and photo-thermal therapeutic activities as well as magnetic resonance (MR) imaging were eventually tested in human cervical cancer (HeLa) cells to validate the assembled flakes as theranostic nanoplatforms.

As shown in Fig. 2, the single-pass incorporation between IDGO and DOX (or DOX-PEG) was examined using a scanning mobility particle sizer (SMPS, 3936, TSI, USA) by measuring the size distributions of flowing particles in the gas-phase. All distributions were unimodal even for the IDGO@DOX and IDGO@DOX-PEG cases, implying that DOX or DOX-PEG was well-merged with IDGO during the assembly. The details of the size distributions [geometric mean diameter (GMD), geometric standard deviation (GSD), and total number concentration (TNC)] are noted, shown in the inset of Fig. 2. The GMD was 108.9 nm for IDGO, which increased to 115.9 nm for IDGO@DOX and to 121.3 nm for IDGO@DOX-PEG because of DOX and DOX-PEG incorporations. Even though there were differences between GMD and TNC, no evident shifts have arisen. The GSD was preferably decreased, suggesting that incorporating DOX or DOX-PEG did not induce great morphological changes of IDGO probably because of the tight conjugation between IDGO and DOX (or DOX-PEG). The sizes of all samples were smaller than 200 nm to secure the nanoscale benefits for efficient nanomedicine,¹⁸ resulting from the size of the precursor particles (*i.e.*, CEI, as shown in Fig. S2, ESI†).

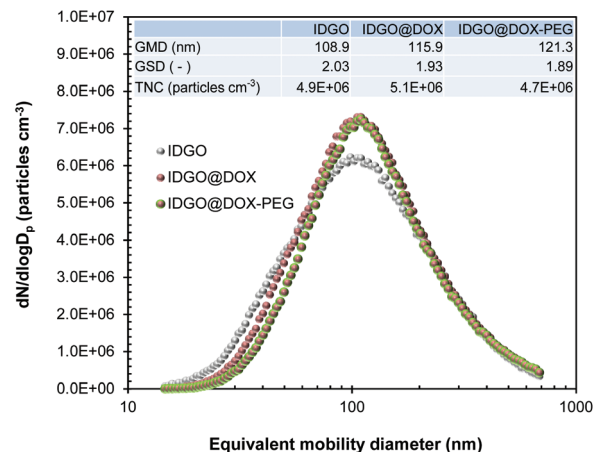


Fig. 2 Size distributions of IDGO@DOX-PEG nanoflakes, including IDGO and IDGO@DOX nanoflakes. Summaries (GMD, GSD, and TNC) of the distributions are also displayed as an inset. No additional distributions are shown in the IDGO@DOX and IDGO@DOX-PEG flakes, which implies that DOX or DOX-PEG was successfully conjugated during the assembly.

Employing CEI nanoparticles (108.4 nm, GMD) can simultaneously supply precursors both for lateral nanoscaled graphitic layers and iron nanoparticles. The designed process, thus, not only provides a suitable platform to assemble composite GO but also confers a beneficial size as well.

Transmission electron microscope (TEM, G2 F20 S-TWIN, Tecnai, USA) was carried out to verify the assembly of IDGO and DOX-PEG incorporated IDGO. The left image of Fig. 3a shows a dotted nanosheet, and the high-magnification images (right-side) reveal the lattice fringe with an interplanar distance of 0.202 nm corresponding to the (110) α -Fe crystal-line facets of body-centered cubic iron. More importantly, high-resolution TEM measurement also shows another lattice fringe spacing of 0.341 nm corresponding to the (002) plane of graphite, confirming the presence of GO. This result supports that the re-construction of CEI into IDGO from the assembly may be greatly extended for preparing different GO composite combinations because spark ablation was used to produce different metal core and graphitic shell configurations.^{19,20} The formation of GO from CEI particles was also confirmed (Fig. S3a, ESI†) using X-ray photoelectron spectroscopy (XPS, K-Alpha, Thermo Scientific, USA), and zero valent iron particles were also verified (Fig. S3b, ESI†). The XPS measurement further demonstrated the existence of FeOOH particles (also confirmed using TEM;²¹ Fig. S3c, ESI†), which may originate from reactions between Fe^{3+} ions and OH^{\cdot} radicals during the ultrasound irradiation. The thermogravimetric analysis (TGA) curve of IDGO exhibited a weight loss probably due to pyrolysis of labile oxygen-containing groups (at 150–400 °C, Fig. S3d, ESI†), while CEI did not show a significant loss because of oxygen free nature (inset of Fig. S3d, ESI†). The dot-removed (inset of the left TEM image) sample showed a transparent sheet of individual GO having wrinkle contrast at the edges. The mean sizes of the IDGO and GO samples were smaller

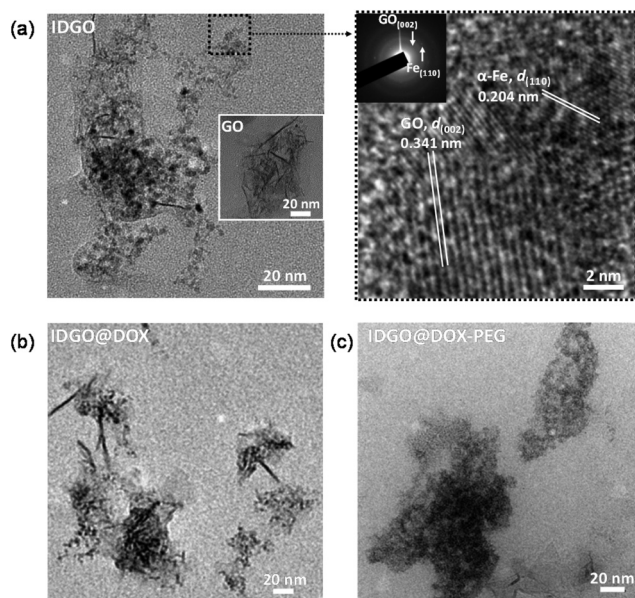


Fig. 3 TEM images of (a) IDGO, (b) IDGO@DOX, and (c) IDGO@DOX-PEG nanoflakes. Low- and high-magnification TEM images, including electron diffraction of IDGO flakes support decoration of iron nanoparticles on GO surfaces. Further incorporation with DOX or DOX-PEG shows different contrasts, supporting the successful conjugation of DOX or DOX-PEG on GO surfaces.

than 150 nm in lateral dimension, supporting that the designed process [*i.e.*, ultrasound treatment (150 W) pulverized graphitic layers into smaller lateral sizes similar to that of a previous report²²] was suitable to assemble fully nanoscale IDGO flakes. The microstructure of IDGO flakes was further confirmed in scanning tunneling microscopy (STM, Nanoscope®IIIa ECSTM, Digital Instruments, USA), as shown in Fig. S4 (ESI†). Fe particles on graphitic layers (approximately 1 nm thickness) were detected, proving restructuring of Fe cores and graphitic shells from CEI particles. Because of direct gas-phase IDGO deposition on a substrate, there were loose bindings between the IDGO and substrate as Moiré pattern indicated.²³ Fig. S5 (ESI†) shows the morphology of the precursor CEI particles, which had iron core and graphitic shell constructed from catalytic graphitization between molten iron and graphite during co-condensation through nitrogen gas flow.²⁴ The revolution of the carbonaceous structure (Fig. S6, ESI†) measured using a Raman spectrometer (XploRA Plus, Horiba, Japan) from graphitic carbon (GC) to CEI confirms the presence of modified (stacked, folded, and nitrated) carbon layers.²⁵ In particular, the spectrum of CEI particles only exhibited a band at around 1280 cm⁻¹, which matched to C–N stretching mode²⁶ due to N incorporation (refer to Fig. S3d, ESI†) from nitrogen gas near the high temperature (~6000 °C) spark channel. The ultrasonic treatment of CEI particles (N-doped) in K₂FeO₄ + H₂O₂ solution to form IDGO further changed the carbonaceous structure, which yielded the D and G bands of carbonaceous structure. Fig. 3b and c (ESI†) show continuous electron dense regions on the basal plane of IDGO,

and discrete iron particles cannot be clearly distinguished. This result demonstrates that DOX or DOX-PEG was deposited through the free interparticle spaces on IDGO *via* electrostatic conjugation between the opposite charges of GO and DOX during solvent extraction of the hybrid droplets (*i.e.*, IDGO + DOX or IDGO + DOX-PEG). The DOX incorporated IDGO samples clearly showed C–O bending (1400 cm⁻¹) and C=O stretching (1740 cm⁻¹) in Fourier transform infrared (FTIR, iS-10, Thermo Electron, USA) measurements (Fig. S7, ESI†), confirming the DOX conjugation on IDGO surfaces. Broad flat spectra were shown in GC and CEI particles, implying that those particles did not have significantly oxygen-containing groups.^{27,28} The decrease in DOX intensity for IDGO@DOX-PEG suggested that DOX on IDGO may be surrounded by long-chained PEG moieties. This result corresponds to changes in zeta potential (Nano ZS90, Malvern Instruments, UK), where the positive potentials for IDGO@DOX decreased when PEG was further added (*i.e.*, IDGO@DOX-PEG; Fig. S8, ESI†). The DOX conjugation was further confirmed by UV-vis spectroscopy (T60, PG Instruments, UK), which revealed the characteristic absorbance of DOX at around 480 nm for IDGO@DOX and IDGO@DOX-PEG, and IDGO only showed broadband absorbance (Fig. S9, ESI†).

The amounts of DOX loaded onto IDGO@DOX and IDGO@DOX-PEG were determined by extracting the drug with dimethyl sulfoxide by ultrasonication followed by quantitation using UV-vis spectrophotometry (U-2800, PerkinElmer, Japan). The loading capacities of IDGO@DOX and IDGO@DOX-PEG were found to be 38 w/w% and 22 w/w%, respectively. The DOX release profile of IDGO@DOX-PEG as shown in Fig. 4a was compared with DOX-PEG. DOX-PEG showed burst release to >60% within 1 h because of the hydrophilic nature of DOX-PEG, although DOX-PEG was a dried formulation through Collision atomization and subsequent solvent extraction. The IDGO@DOX-PEG nanoflakes showed a controlled release feature because DOX was firmly bound onto IDGO *via* electrostatic interaction as well as π - π^* stacking.²⁹ The cumulative DOX release from both samples was approximately 10% higher (showing pH-dependent release) in acidic medium [acetate-buffered saline (ABS, pH 5.8)] than that in phosphate-buffered saline (PBS, pH 7.4) because of rapid protonation of amine groups in acidic pH. IDGO@DOX-PEG and DOX-PEG were further used to evaluate and quantify the intracellular uptake by HeLa cells through fluorescence-activated cell sorting (FACS, BD Biosciences, USA; Fig. 4b) and fluorescent microscopy (Eclipse Ti, Nikon, Japan) studies (Fig. 4c). FACS analyses showed the incubation time-dependent (2 and 6 h) cellular internalization of both samples. The fluorescent signals of DOX from DOX-PEG for both incubation times were greatly larger than those from IDGO@DOX-PEG possibly because of controlled DOX release characteristics from conjugation between IDGO and DOX. The controlled DOX release was further compared with DOX-PEG conjugated with lateral microdimensional GO (LGO@DOX-PEG; Fig. S10a, ESI†) flakes to validate a capability for DOX conjugation of fully nanoscale

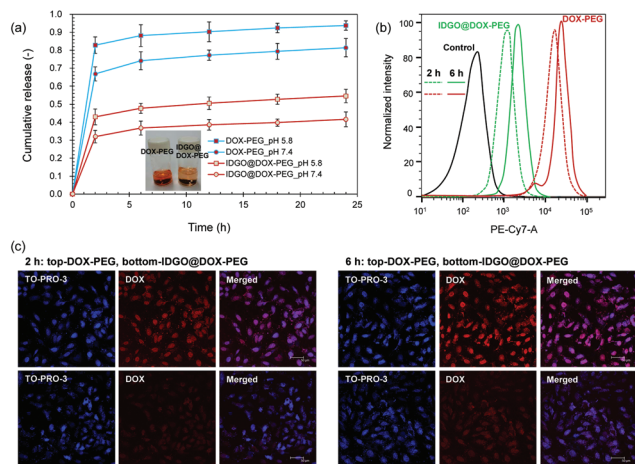


Fig. 4 DOX release characteristics from IDGO@DOX-PEG nanoflakes, including the DOX-PEG platform for comparison purposes. The conjugation of DOX with IDGO flakes greatly suppressed burst DOX releases compared to the DOX-PEG platform. (a) *In vitro* DOX release at pH 5.8 (ABS) and pH 7.4 (PBS). Insets show the DOX-PEG solution and IDGO@DOX-PEG dispersion. The difference in color was due to the DOX conjugation on the IDGO surfaces. (b) FACS measurements for cellular uptake of DOX from IDGO@DOX-PEG and DOX-PEG using HeLa cells as a function of incubation time. (c) Fluorescent microscope images of HeLa cells following 2 and 6 h of incubation of IDGO@DOX-PEG and DOX-PEG. TO-PRO-3 was used for staining the nucleus.

GO flakes. As shown in Fig. S10b (ESI[†]), IDGO@DOX-PEG showed a controlled release feature even better than that from LGO@DOX-PEG, which proved that a fully nanoscale structure is more suitable for controlled DOX release. Fluorescent microscopy studies were carried out after 2 and 6 h of incubations to confirm that IDGO@DOX-PEG flakes were properly internalized (Fig. 4c). Time-dependent DOX release could be seen in both samples, and the fluorescent DOX signal was superimposed with nuclear stain (TO-PRO-3). Evidently large

red fluorescence at 2 and 6 h post-incubation for DOX-PEG represented burst DOX releases, and the bursting was efficiently avoided in the case of IDGO@DOX-PEG, corresponding to the FACS results. According to the FACS and fluorescent microscopy studies, it can be concluded that the assembled IDGO was feasible to bind with the DOX molecules *via* the electrostatic interaction between the -COO^- groups (plane and edge sites) and protonated amine groups. Thus, it may be an alternative to resolve burst drug release as well as limited internalization modes for lateral microdimensional GO (*i.e.*, mostly phagocytosis).³⁰

The magneto- and photo-thermal effects of IDGO nanoflakes were tested in PBS (at 1 mg mL^{-1} for magneto-thermal and at $100 \text{ }\mu\text{g mL}^{-1}$ for photo-thermal) as a function of exposure time. As shown in Fig. 5a, the temperature of IDGO dispersion increased up to 49°C after 5 min and plateaued at around 51°C under a continuous alternating magnetic frequency (AMF). Such temperature elevation originated from the magnetization of GO ($M_s = 11.8 \text{ emu g}^{-1}$) through automatic iron nanoparticle decoration during the assembly (Fig. S11, ESI[†]), and the M_s value was within $7\text{--}22 \text{ emu g}^{-1}$, which is known as sufficient for bioapplication.³¹ In the case of near-infrared (NIR) irradiation, IDGO dispersion showed a linear correlation between irradiation time and temperature, reaching $>60^\circ\text{C}$ after 10 min (*cf.* 47°C after 5 min). The elevated temperatures after 5 min (AMF and NIR exposure) are sufficient to induce hyperthermia at the tumor region to inhibit the regulatory and proliferative processes of cancerous cells.³⁰ Before evaluating the hyperthermia activities, the cytotoxicities of IDGO nanoflakes were first measured in HeLa cells by a 3-(4,5-dimethylthiazol-2-yl)-2,5-diphenyltetrazolium bromide (MTT) assay after 24 h of incubation using a medium containing different concentrations of IDGO. As shown in Fig. 5b, an increasing concentration of IDGO did not greatly alter cell proliferation and viability, which consistently remained at about 100% of PBS-only-treated control. This result suggests the biocompatibility and negligible cytotoxicity

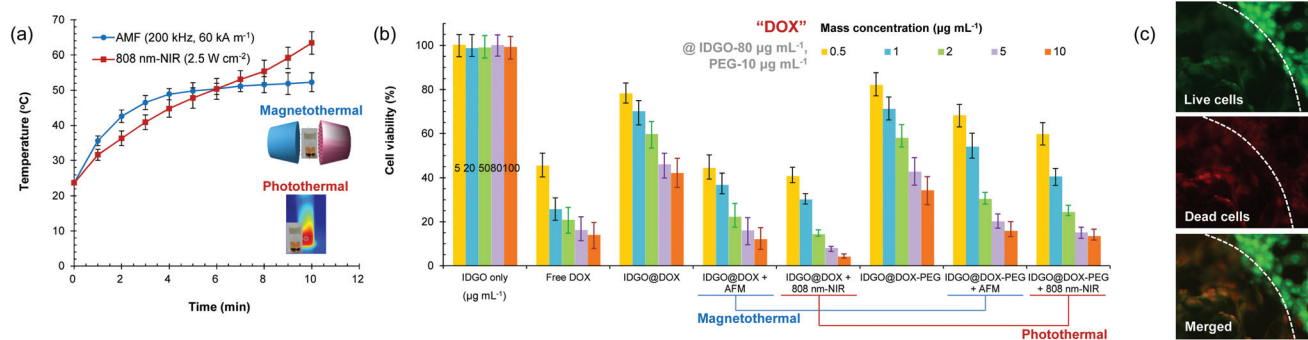


Fig. 5 *In vitro* therapeutic effects of IDGO@DOX-PEG nanoflakes, including IDGO@DOX and free DOX. (a) Magneto- and photo-thermal temperature elevation of IDGO@DOX-PEG dispersion as a function of irradiation time. The results demonstrate both magnetic and optical reactivities of the flakes. (b) Viabilities of HeLa cells as a function of the DOX amount in IDGO@DOX and IDGO@DOX-PEG flakes with or without AMF and NIR exposures following 24 h of incubation. IDGO did not show significant cytotoxic effects at the chosen concentrations, and DOX incorporation and hyperthermic effects of IDGO induced cytotoxicities. (c) Representative live/dead assay after NIR irradiation (2 min, $50 \text{ }\mu\text{g mL}^{-1}$) with IDGO@DOX-PEG. The results supported the hyperthermic effect of IDGO@DOX-PEG.

of IDGO flakes because of their fully nanoscale feature, which may also be related to the strong attachment of iron particles on GO. Thus, IDGO flakes could not undergo endosomal or phagosomal escape to the cytoplasm and mitochondria. On the other hand, free DOX and DOX-incorporated IDGO (*i.e.*, IDGO@DOX and IDGO@DOX-PEG) flakes exhibited dose-dependent cytotoxicities with increasing DOX concentration from 0.5 to 10 $\mu\text{g mL}^{-1}$. The cell viabilities further decreased when the cells were incubated with IDGO@DOX or IDGO@DOX-PEG upon 5 min of AMF or 2 min of NIR exposure, which were thus comparable to free DOX because of the resultant heat induction (*i.e.*, inducing chemosensitization and increased release of DOX). The live/dead assay results (Fig. 5c) from 2 min NIR exposure further supported that hyperthermia using IDGO@DOX-PEG can be site selectively applied to kill cancer cells without harming adjacent healthy cells. In addition, IDGO@DOX-PEG flakes were incubated with L929 (mouse fibroblast) and human nasal epithelial (HNEp) cells to assess cytotoxic effects on normal cells (Fig. S12, ESI†). The IDGO flakes did not induce significant cytotoxic effects on the cells at the chosen concentrations, and IDGO@-PEG flakes exhibited lower cytotoxic effects on the cells compared with the effects on HeLa cells. This implies that base IDGO flakes are also biocompatible on normal cells as well as the lower cytotoxic effects of IDGO@DOX-PEG flakes on normal cells are attributable to the smaller uptake of IDGO@DOX-PEG flakes (Fig. 4b) that induces the slow release of DOX from the flakes.

Considering magnetic field reactivity, IDGO@DOX-PEG nanoflakes were further employed to confirm their ability as an MR imaging contrast agent in a theranostic nanoplatform. The results (Fig. 6) show the inverse relaxation time ($1/T_2$) of IDGO@DOX-PEG as a function of equivalent iron concentration.³² As shown in the inset of Fig. 6, T_2 -weighted images of HeLa cells labeled by IDGO@DOX-PEG nanoflakes were acquired over the equivalent Fe concentration of 0 to 20 $\mu\text{g mL}^{-1}$ using a 3.0 T MR imaging scanner (Achieva 3.0 T TX, Philips, Netherlands). The resulting MR images show that IDGO@DOX-PEG induced a hypointense (negative in bright-

ness for the T_2 -weighted image) signal in a concentration-dependent manner after 3 h of incubation. The negative signal was due to the local perturbation field induced by IDGO@DOX-PEG, which caused an evident shortening of proton relaxation time (T_2 relaxation time) during the MR imaging process.³³ It can be suggested that the automatic decoration during the ultrasound irradiation of CEI particles could also facilitate MR imaging. The present work, thus, may be a stepping stone developing a realizable system for an efficient production of theranostic composite GO nanosystems.

In the light of mass and energy balances, lastly, the production rate and specific energy consumption (SEC) of IDGO@DOX-PEG flakes were respectively found to be 0.058 g h^{-1} and 0.78 kW h g^{-1} from a single-channel spark ablation, which are greater than other spark ablation material production systems.³⁴ On the other hand, a greater SEC of this approach than an eco-friendly graphene production (0.025 kW h g^{-1})³⁵ needs improvements in SEC of spark ablation, although most spark ablations do not require electrode cooling facilities and vacuum conditions. Employing arc ablation instead of spark ablation to produce CEI particles might be a plausible alternative because the arc exhibited comparable SECs (0.014–0.022 kW h g^{-1})³⁴ with the previous report.³⁵

Conclusions

The designed single-pass process was suitable to continuously assemble a fully nanoscale GO composite without any process interruptions. The assembled flakes showed biocompatibility, drug loading capacity, and photothermal activity. Automatic iron decoration on GO surfaces in the course of assembly further facilitated chemo-magnetotherapy and MR imaging, suggesting that the single-pass process may provide conceptual leaps in theranostic nanosystem preparation. In particular, the dual hyperthermic effect might breakthrough limited NIR penetration (for deep-seated tumors) and heating efficiency (owing to thermal bystander effect) and offer multiple hyperthermia cycles. Employing CEI nanoparticles and $\text{K}_2\text{FeO}_4 + \text{H}_2\text{O}_2$ solution enabled a simple and green assembly of fully nanoscale IDGO. This study may also open up possibilities to assemble various configurations of metal-decorated GO nanoflakes by applying different metal rods at the spark ablation to supply the desired carbon-encapsulated metal nanoparticles. Therefore, the designed assembly can not only offer a realizable continuous production platform but also provide a fully nanoscale configuration and prepare metallic nanoparticle-decorated GO composites for numerous theranostic and other technological (*e.g.*, catalysis, energy, electronics, and environment) applications.

Conflicts of interest

There are no conflicts to declare.

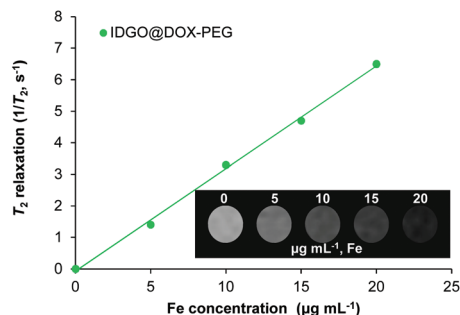


Fig. 6 *In vitro* MR imaging using IDGO@DOX-PEG nanoflakes. The T_2 relaxation rate increased with increasing iron concentration. Inset shows T_2 -weighted MR imaging of IDGO@DOX-PEG-incubated cells as a function of Fe concentration. The results verify that iron decoration on the flakes gives functionality as a contrast agent for MR imaging. IDGO@DOX-PEG flakes, thus, are suitable nanoplatforms for theranostics.

Acknowledgements

This work was supported by the Creative Economy Leading Technology Development Program through the Gyeongsangbuk-Do and Gyeongbuk Science & Technology Promotion Center of Korea (SF316001A). This work was also supported by the 215A356002 Yeungnam University Research Grant.

Notes and references

- V. Georgakilas, J. N. Tiwari, K. C. Kemp, J. A. Perman, A. B. Bourlinos, K. S. Kim and R. Zboril, *Chem. Rev.*, 2016, **116**, 5464.
- K. Muazim and Z. Hussain, *Mater. Sci. Eng., C*, 2017, **76**, 1274.
- K. Yang, L. Feng and Z. Liu, *Adv. Drug Delivery Rev.*, 2016, **105**, 228.
- Y. Zhu, S. Murali, W. Cai, X. Li, J. W. Suk, J. R. Potts and R. S. Ruoff, *Adv. Mater.*, 2010, **22**, 3906.
- F. Yin, B. Gu, Y. Lin, N. Panwar, S. C. Tjin, J. Qu, S. P. Lau and K.-T. Yong, *Coord. Chem. Rev.*, 2017, **347**, 77.
- G. Gollavelli and Y.-C. Ling, *Biomaterials*, 2012, **33**, 2532.
- X.-D. Li, X.-L. Liang, X.-L. Yue, J.-R. Wang, C.-H. Li, Z.-J. Deng, L.-J. Jing, L. Lin, E.-Z. Qu, S.-M. Wang, C.-L. Wu, H.-X. Wu and Z.-F. Dai, *J. Mater. Chem. B*, 2014, **2**, 217.
- H. Wang and S. Zhou, *Biomater. Sci.*, 2016, **4**, 1062.
- C. Cheng, S. Li, A. Thomas, N. A. Kotov and R. Haag, *Chem. Rev.*, 2017, **117**, 1826.
- G. Shi, S. Araby, C. T. Gibson, Q. Meng, S. Zhu and J. Ma, *Adv. Funct. Mater.*, 2018, **28**, 1706705.
- Y. Chen, L. Wang and J. Shi, *Nano Today*, 2016, **11**, 292.
- W. J. Park, Y. Yoon, S. Kim, S. Y. Choi, S. Yoo, Y. Do, S. Jung, D. H. Yoon, H. Park and W. S. Yang, *ACS Omega*, 2017, **2**, 186.
- G. Reina, J. M. González-Donminguez, A. Criado, E. Vázquez, A. Bianco and M. Prato, *Chem. Soc. Rev.*, 2017, **46**, 4400.
- K. Yang, L. Feng, H. Hong, W. Cai and Z. Liu, *Nat. Protoc.*, 2013, **8**, 2392.
- Y. Zhou, X. Jing and Y. Chen, *J. Mater. Chem. B*, 2017, **5**, 6451.
- J. H. Byeon and Y.-W. Kim, *Nanoscale*, 2012, **4**, 6726.
- K. Muthoosamy and S. Manickam, *Ultrason. Sonochem.*, 2017, **39**, 478.
- N. Desai, *AAPS J.*, 2012, **14**, 282.
- J. H. Byeon and J.-W. Kim, *ACS Appl. Mater. Interfaces*, 2010, **2**, 947.
- J. H. Byeon and J.-W. Kim, *Appl. Phys. Lett.*, 2010, **96**, 153102.
- T. P. Almeida, M. W. Fay, Y. Zhu and P. D. Brown, *Nanoscale*, 2010, **2**, 2390.
- C. Cai, N. Sang, Z. Shen and X. Zhao, *J. Exp. Nanosci.*, 2017, **12**, 247.
- K. Gotterbarm, C. Steiner, C. Bronnbauer, U. Bauer, H.-P. Steinrück, S. Maier and C. Papp, *J. Phys. Chem. C*, 2014, **118**, 15934.
- J. H. Byeon, J. H. Park, K. Y. Yoon and J. Hwang, *Nanoscale*, 2009, **1**, 339.
- C. Giordano, A. Kraupner, I. Fleischer, C. Henrich, G. Klingelhöfer and M. Antonietti, *J. Mater. Chem.*, 2011, **21**, 16963.
- M. R. Wixom, *J. Am. Ceram. Soc.*, 1990, **73**, 1973.
- S. A. El-Khodary, G. M. El-Enany, M. El-Okr and M. Ibrahim, *Electrochim. Acta*, 2014, **150**, 269.
- A. Kasprzak, A. M. Nowicka, J. P. Sek, M. Fronczak, M. Bystrzejewski, M. Koszytkowska-Stawinska and M. Poplawska, *Dalton Trans.*, 2018, **47**, 30.
- A. M. Panich, A. I. Shames, M. I. Tsindlekht, Y. Yu. Osipov, M. Patel, K. Savaram and H. He, *J. Phys. Chem. C*, 2016, **120**, 3042.
- Q. Mu, G. Su, L. Li, B. O. Gilbertson, L. H. Yu, Q. Zhang, Y. P. Sun and B. Yan, *ACS Appl. Mater. Interfaces*, 2012, **4**, 2259.
- Q. L. Fan, K. G. Neoh, E. T. Kang, B. Shuter and S. C. Wang, *Biomaterials*, 2007, **28**, 5426.
- S. Brulé, M. Levy, C. Wilhelm, D. Letourneur, F. Gazeau, C. Ménager and C. Le Visage, *Adv. Mater.*, 2011, **23**, 787.
- F. Sousa, B. Sanavio, A. Sacconi, Y. Tang, I. Zucca, T. M. Carney, A. Mastropietro, P. H. Jacob Silva, R. P. Carney, K. Schenk, A. O. Omrani, P. Huang, L. Yang, H. M. Rønnow, F. Stellacci and S. Krol, *Bioconjugate Chem.*, 2017, **28**, 161.
- M. Slotte and R. Zevenhoven, *Energies*, 2017, **10**, 1605.
- A. R. Kamali, *Green Chem.*, 2016, **18**, 1952.